A R C H I V E S O F M E T A L L U R G Y A N D M A T E R I A L S
Volume 54 2009 Issue 4

K. OSIŃSKA*, J. MASZYBROCKA*, J. PLEWA**, D. CZEKAJ*

FABRICATION AND DIELECTRIC PROPERTIES OF SOL-GEL DERIVED (Ba,Sr)TiO_3 CERAMICS

OTRZYMYWANIE I WŁAŚCIWOŚCI DIELEKTRYCZNE CERAMIKI (Ba,Sr)TiO_3 OTRZYMANEJ METODĄ ZOLOWO-ŻELOWĄ

The $(Ba_{1-x}Sr_x)TiO_3$ ceramic solid solution in the range $0.3 \leqslant \times \leqslant 0.5$ was prepared by the sol-gel method. Barium acetate, strontium acetate and tetra-butyl titanate were used as starting materials. Thermal evolution of the dried gel as well as ceramic powder was studied by simultaneous thermal analysis. The amorphous gel of BST was calcined in the furnace and pressed into pellets. The compacts were next sintered by free sintering method at temperature T=1450°C. The structure, microstructure and dielectric properties were studied for sol-gel derived ceramics.

Keywords: Barium strontium titanate ceramics, sol-gel method, dielectric properties

Ceramiczny roztwór stały $(Ba_{1-x}Sr_x)TiO_3$ w zakresie x=0,3-0,5 otrzymany został metodą zolowo-żelową. Jako materiały wyjściowe zastosowano: octan baru, octan strontu i n-butanolan tytanu. Dla suchego żelu w postaci proszku ceramicznego przeprowadzono analizę termiczną. Amorficzny żel poddano kalcynacji w piecu i prasowany w dyski. Próbki były następnie spiekane swobodnie w temperaturze T=1450°C. Określono układ krystalograficzny, grupę przestrzenną i parametry komórki elementarnej otrzymanej metodą zolowo-żelową ceramiki BST oraz zbadano jej mikrostrukturę i właściwości dielektryczne.

1. Introduction

Barium titanate ($BaTiO_3$) is known as a typical ferroelectric material, which exhibits three sharp transitions: a first-order ferroelectric-paraelectric phase transition (cubic-tetragonal) around T=130°C (also called Curie temperature T_C), a tetragonal-orthorhombic phase transition around T=50°C and an orthorhombic-rhombohedral phase transition around T=-80°C [1]. With partial substitution of the titanium by other tetravalent ions like in Ba(Ti,Sn)O_3, Ba(Ti,Zr)O_3 and Ba(Ti,Ce)O_3 etc., the variation of the permittivity around the Curie temperature T_C was found to get smeared out in both ceramics and single crystal specimens, i.e. to exhibit diffuse phase transition (DPT), a similar behaviour to well known complex lead perovskite ferroelectric relaxors.

The conventional method of synthesizing (Ba,Sr)TiO_3 powder relies on solid-state reaction at a high temperature of around T=1200°C. High-temperature (Ba,Sr)TiO_3 powders due to the repetitive calcinations and grinding treatments, and lower chemical activity are not suitable for preparation of fine grained (Ba,Sr)TiO_3 ceramics [2]. The new emerging sol-gel methods present some particular advantage in obtaining the (Ba,Sr)TiO_3 powder with high purity and homogeneity, through a lower temperature process, avoiding contamination of the materials. They also yield better stoichiometric control and allow the preparation of dense ceramics. Finally, another important feature of sol-gel processes is the possibility of grain size and grain shape control.

It is worth noting that in today's terminology, sol-gel processing is a form of nanostructure processing. Not only does the sol-gel process begin with a nanometer sized unit, a molecule, it also undergoes reactions on the nanometer scale resulting in a material with nanometer features [3]. Therefore, the present work is devoted to application of the sol-gel processing in fabrication of $Ba_{1-x}Sr_xTiO_3$ (BST) ceramic solid solutions in the range of x from x=0.3 to x=0.5. We also report the results of investigation of dielectric properties, the structure and microstructure of sol-gel derived (Ba,Sr)TiO_3 electroceramics.

* UNIVERSITY OF SILESIA, DEPARTMENT OF MATERIALS SCIENCE, 41-200 SOSNOWIEC, 2 SNIEZNA STR., POLAND
** UNIVERSITY OF APPLIED SCIENCES MÜNSTER, 39, STEGERWALDSTRASSE, STEINFURT, D-48565, GERMANY

2. Experimental

Solid solution $Ba_{1-x}Sr_xTiO_3$ (BST), where x=0.30; 0.35; 0.40; 0.45; 0.50, was obtained by the sol-gel method. Barium acetate ($Ba(CH_3COO)_2$, 99%), strontium acetate ($Sr(CH_3COO)_2$, 99%), and tetra-butyl titanate ($Ti(OC_4H_9)_4$, 97%) were used as starting materials. Glacial acetic acid (CH_3COOH, 99.9%) and butyl alcohol (C_4H_9OH, 99.9%) were used as solvents. After dissolving the barium acetate and strontium acetate in acetic acid at T=100°C for t=0.5h and cooling down to room temperature and after mixing tetrabutyl titanate in butyl alcohol, Ba-Sr solution was mixed with Ti solution by magnetic stirrer for t=0.5h. Acetyloacetone ($CH_3COCH_2COCH_3$) was added as stabilizer, followed by hydrolysis. The sol was relatively stable and became a gel in a few days. The amorphous BST gel was calcined in the furnace at T=850°C for t=4h, milled and pressed into pallets of d=10mm in diameter and h=2mm thick at p=300MPa. The compacts were next sintered by free sintering method at temperature T=1450°C for t=4h.

The density of the sintered samples was measured by the Archimedes method. The specimens were 91-96% of the theoretical (X-ray) density for all compositions.

Thermal analysis was measured by STA-409 Netzsch analyzer. The morphology of BST powder after sintering and milling was observed by transmission electron microscopy.

The crystal structure was examined by X-ray diffraction with CoK_α radiation (Θ-2Θ method, scan step size $\Delta\Theta$=0.02 deg, scan type continuous, scan step time t=4s) at room temperature. The lattice parameters for sol-gel derived BST ceramic specimens were calculated using Rietveld refinement, embedded into the computer program PowderCell 2.4 [4].

Microstructure of the ceramic samples was observed by both optical microscopy and scanning electron microscopy on fractures and polished sections followed by a thermal etching using Olympus BX 60M and Philips XL 30, ESEM/TMP, respectively.

Quantitative analysis of the microstructure of the ceramic samples was carried out with the image analysis software VISILOG 6. The developed algorithm allowed for the successful grain boundary detection. The number of grains was determined by using the Jeffries' method [5]. In this study the mean grain section area and the mean grain chord length have been used as grain-size measures.

For dielectric measurements, sintered samples were polished and silver paste was deposited on both sides. Dielectric permittivity (ε') and loss factor (tgδ) were measured, at different frequencies between f_{min}=10kHz and f_{max}=1MHz, as function of temperature. The impedance analyser of HP4192A type was employed and measurements were carried out during heating up and cooling down at the rate of $1°C \times min^{-1}$ in the temperature range of ΔT=-100°C-120°C.

3. Results and discussion

Figure 1a, 1b, 2a, 2b, 3a, 3b show thermal analysis curves of BST70/30, BST60/40 and BST50/50 dry gels, respectively, before calcination (a) and after calcination (b). One can see from Fig.1a, 2a, and 3a that all dried gel powders exhibited a large total weight loss $\Delta m \approx$44.15% for BST70/30, $\Delta m \approx$ 47% for BST60/40, and $\Delta m \approx$ 46.8% for BST50/50. The analyses show three stages of weight loss.

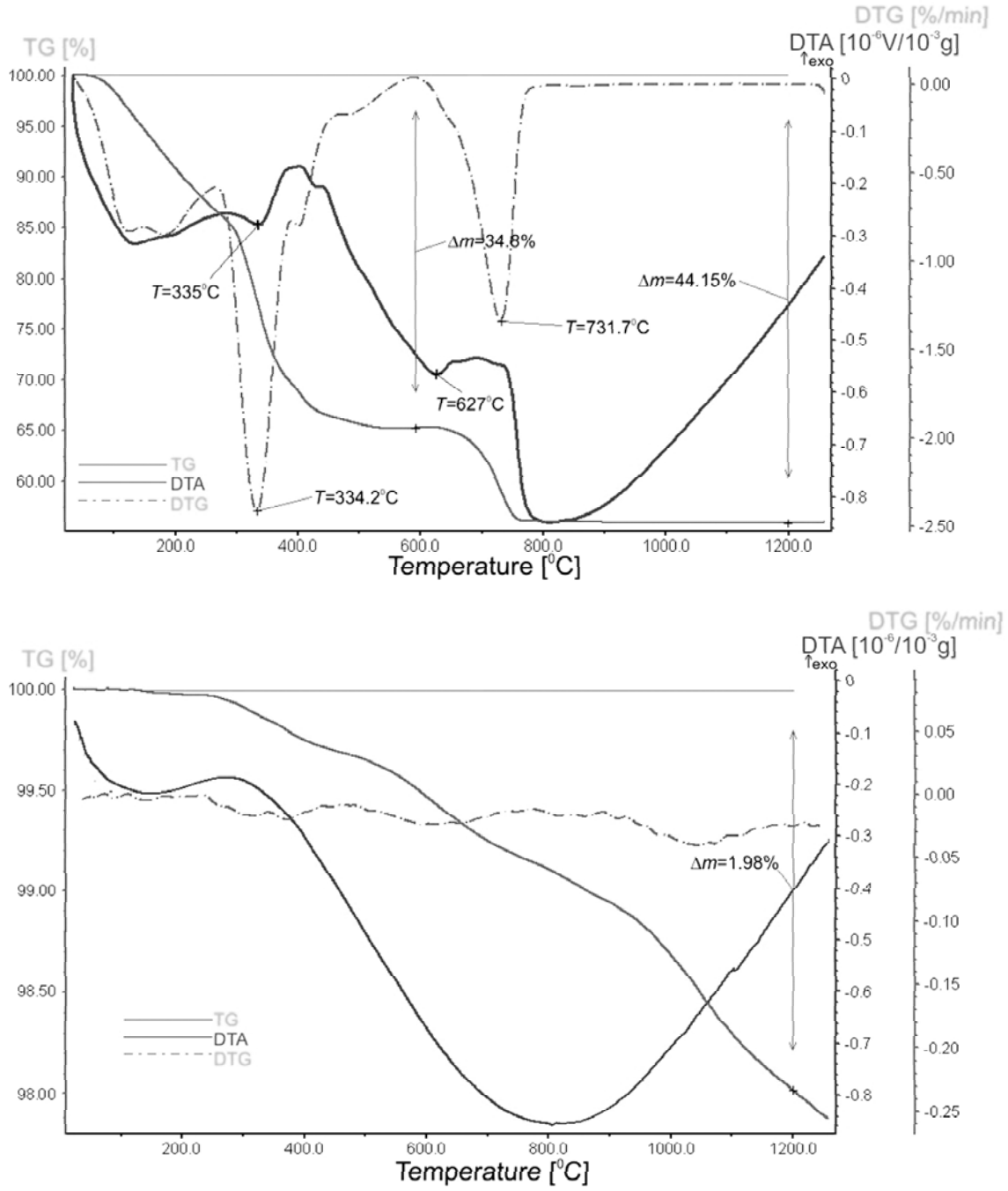

Fig. 1. a) Thermal analysis data of BST70/30 dry gel before calcination. b) Thermal analysis data of BST70/30 dry gel after calcination

The endothermic peak at around T=130°C and corresponding weight loss $\Delta m_1 \approx 16\%$ for BST70/30 on the TG curve, T=120°C and corresponding weight loss $\Delta m_1 \approx 15\%$ for BST60/40 and T=119.2°C and corresponding weight loss $\Delta m_1 \approx 18\%$ for BST50/50 on the TG curve, are due to the evaporation of solvents. Below T=300°C, the first drop corresponds to the evaporation of the solvent.

The second notable weight loss $\Delta m_2 \approx 26\%$ was detected at $T \approx 334$°C for BST70/30, $\Delta m_2 \approx 21\%$ was detected at T=337°C for BST 60/40 and $\Delta m_2 \approx 19.6\%$ was detected at $T \approx 340$°C for BST50/50 which matched a large exothermic peak in the DTA curve. Since no crystallization takes place below T = 500°C, the weight loss is probably due to the decomposition of organic additives in the gel.

The exothermic peak around $T \approx 400$°C and relatively broad exothermic features at $T \approx 650$°C for all dried gels, could be due to crystallization of various intermediate phases. It is known that for sol-gel derived barium titanate several intermediate phases exist prior to the transformation of the amorphous phase into the perovskite phase. The nature of these intermediate phases and the crystallization sequence depends upon the precursors used [6].

The third notable drop between $T = 600$°C and $T = 800$°C corresponds to an endothermic peak of the DTG curve at about $T = 731$°C for BST70/30, $T = 718.5$°C for BST60/40 and $T = 722$°C for BST50/50. The weight loss originates from the release of various side products during alcoxolation and oxolation.

Fig.1b, 2b and 3b show that after calcination no thermal effects take place in BST70/30, BST60/40 and BST50/50 powder.

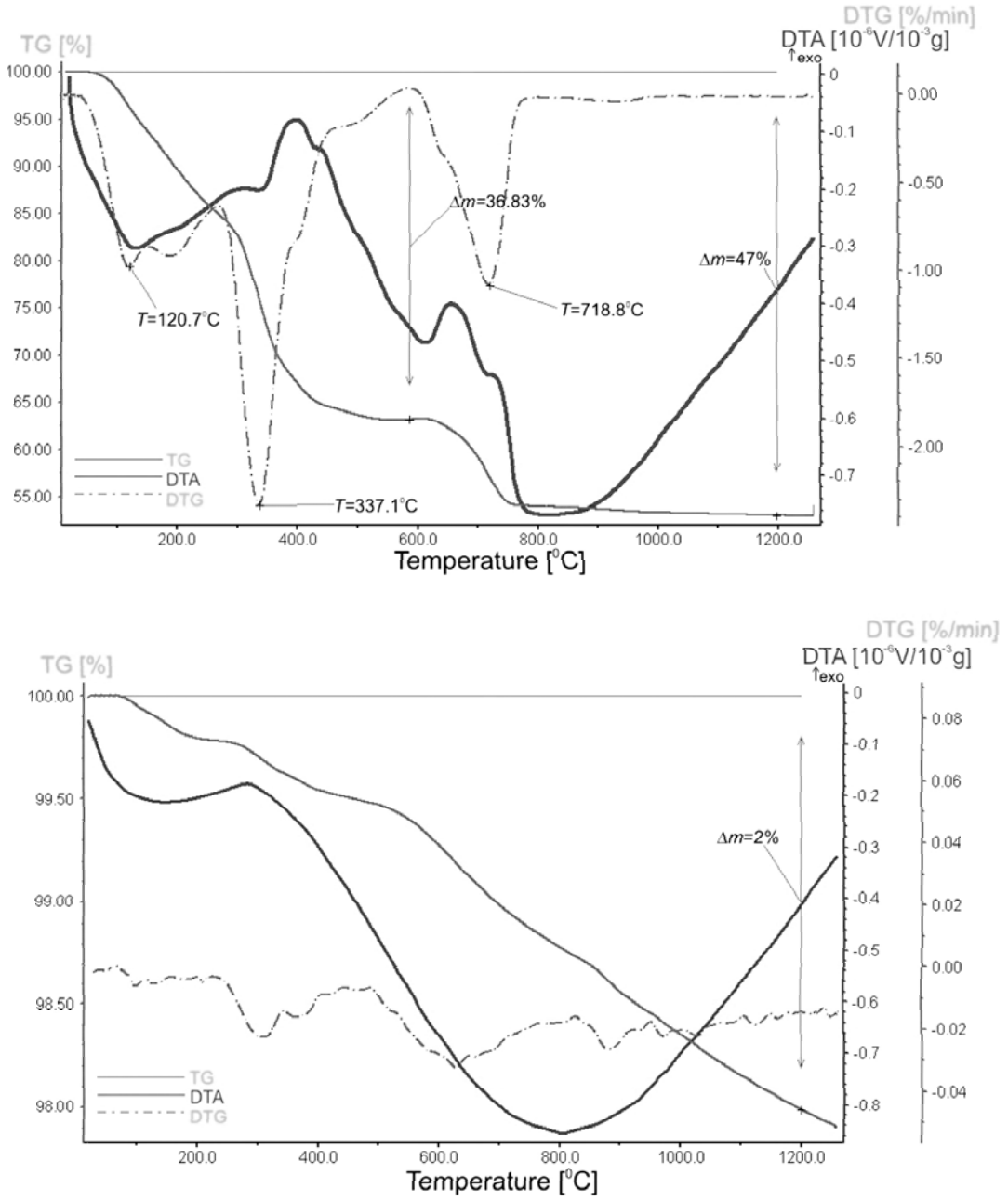

Fig. 2. a) Thermal analysis data of BST60/40 dry gel before calcination. b) Thermal analysis data of BST60/40 dry gel after calcination

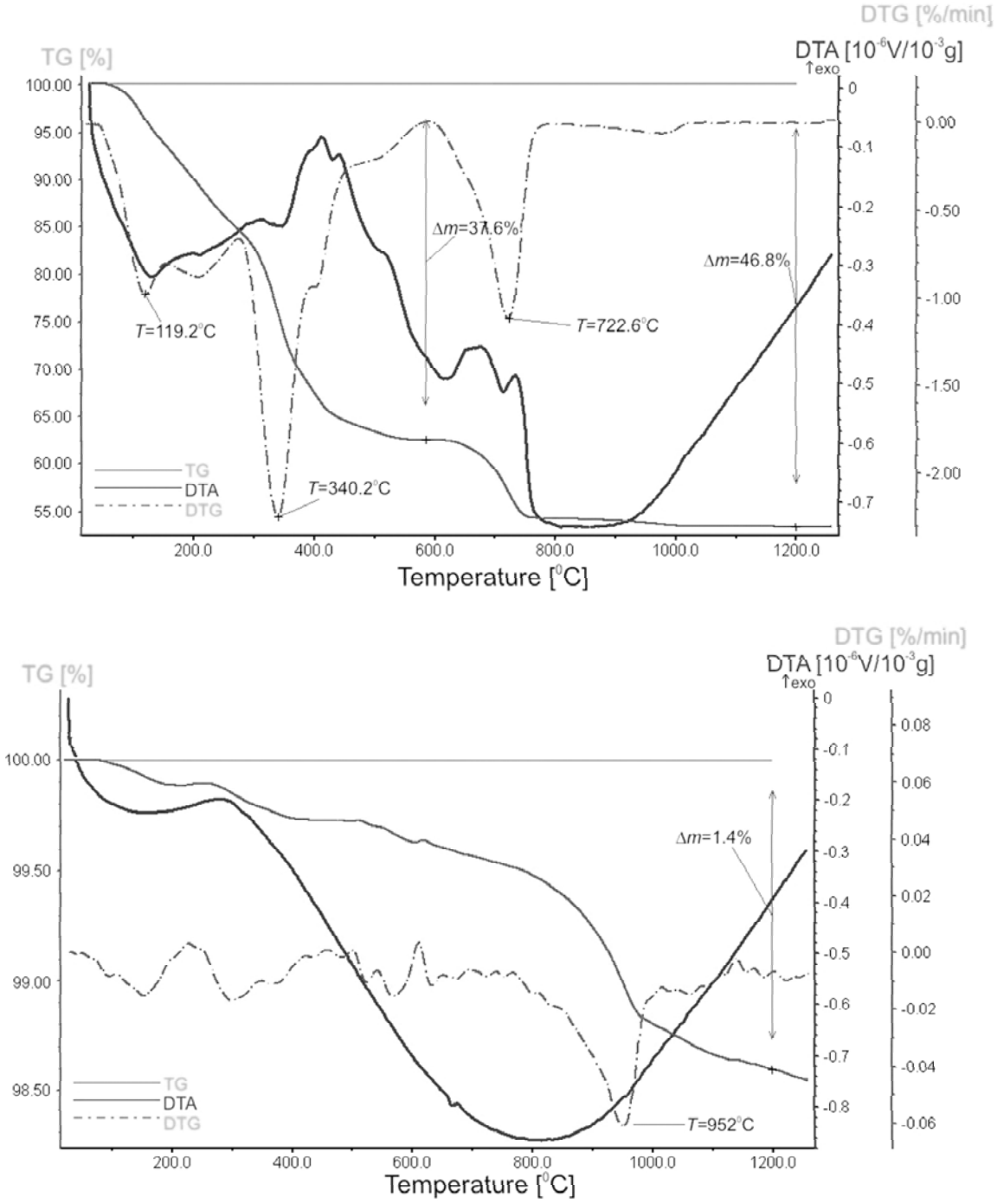

Fig. 3. a) Thermal analysis data of BST50/50 dry gel before calcination, b) Thermal analysis data of BST50/50 dry gel after calcination

On the basis of thermal analysis, the temperature calcination was chosen $T = 850°C$ for all dried gels.

Transmission electron micrographs of $Ba_{1-x}Sr_xTiO_3$ powder for x=0.30; 0.40;0.50 after sintering and milling are presented in Fig.4, Fig.5, Fig.6, respectively.

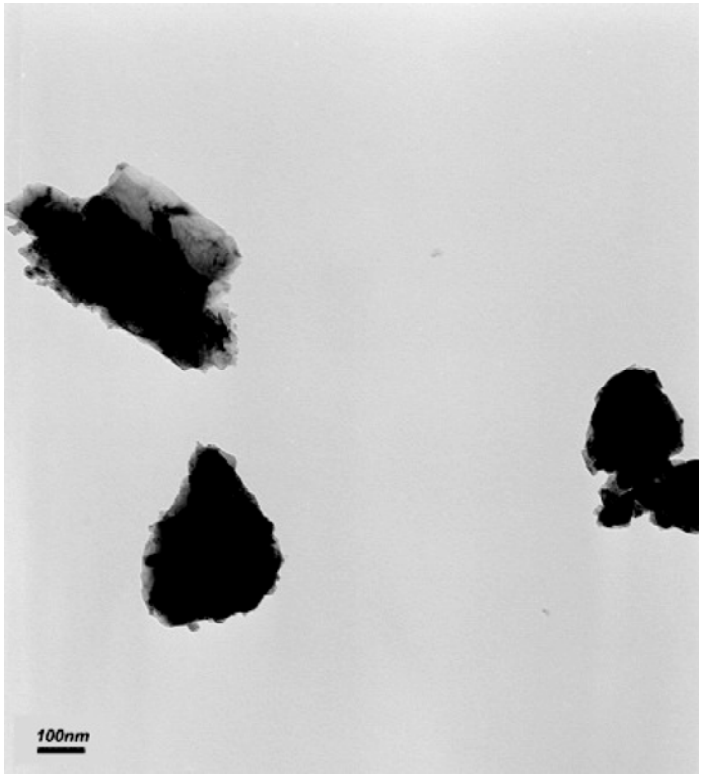

Fig. 4. TEM micrographs of BST70/30 ceramic powder after sintering and milling

Fig. 5. TEM micrographs of BST60/40 ceramic powder after sintering and milling

Fig. 6. TEM micrographs of BST50/50 ceramic powder after sintering and milling

It was found that the powder formed agglomerates in the dispersed solution. It was also observed that the shape of the powder particles was not uniform. In most cases, the primary particles are not isolated, but form wormlike agglomerates with diameters of 300nm and lengths of up to 400nm.

In Fig.7 the microstructure taken by optical microscope is shown whereas Fig.8a shows the SEM image of the microstructure and its binary representation for ceramic sample with x=0.4. Spatial distribution of the grain sizes is also given in Fig.8b.

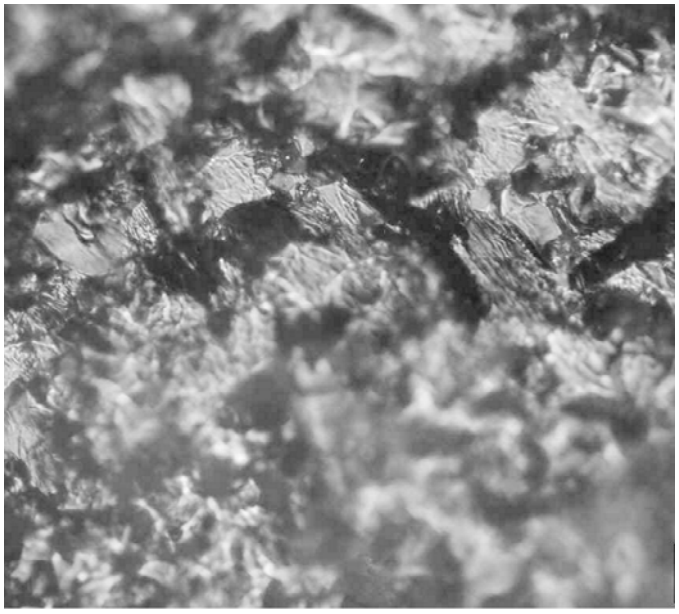

Fig. 7. Optical image for $Ba_{0.6}Sr_{0.4}TiO_3$ ceramics

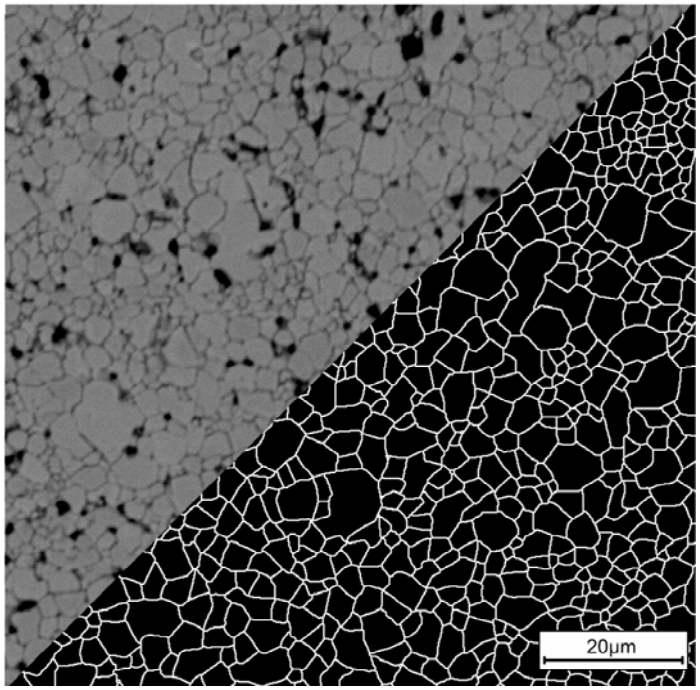

Fig. 8a.) SEM microstructure and its binary representation for $Ba_{0.6}Sr_{0.4}TiO_3$ ceramics

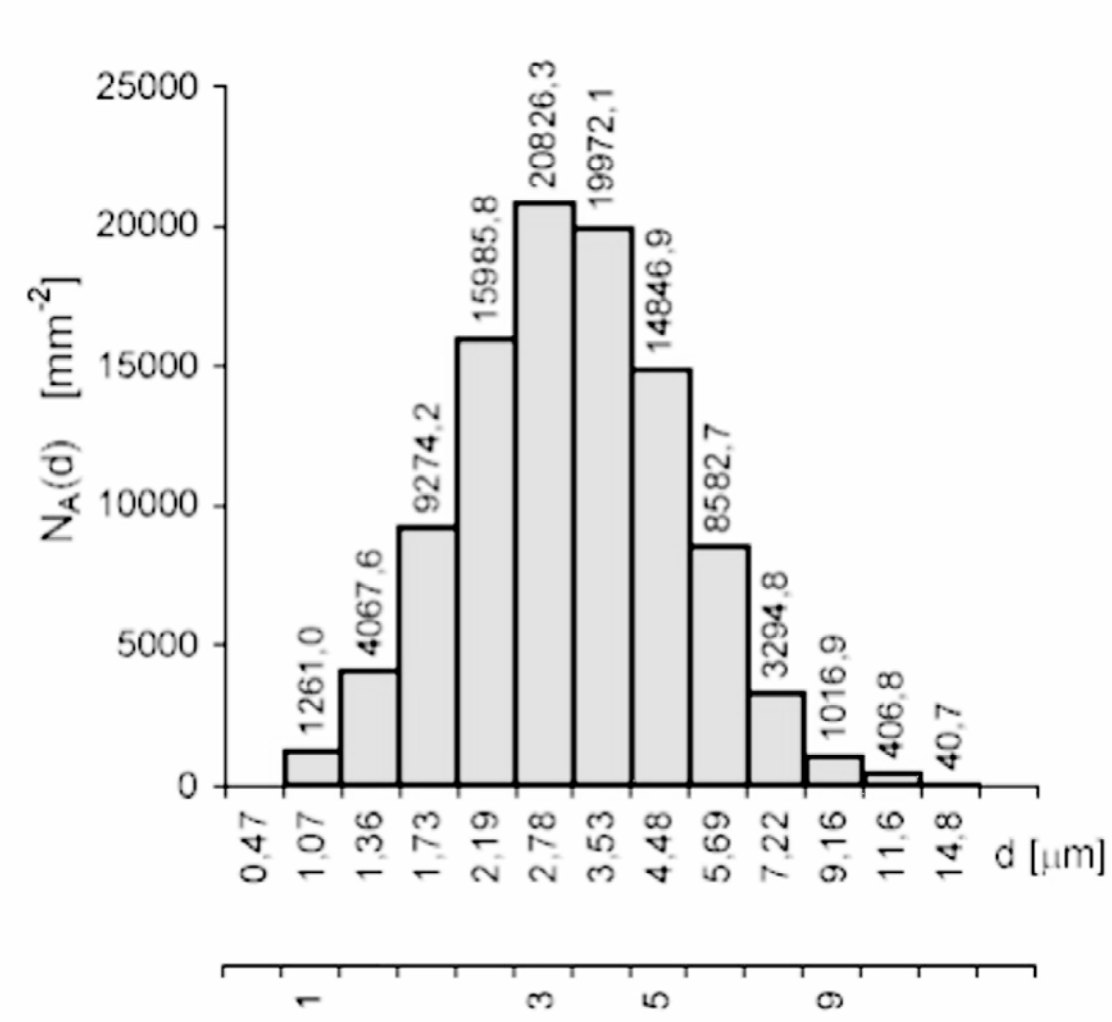

Fig. 8b.) Distribution of the grain sizes of $Ba_{0.6}Sr_{0.4}TiO_3$ ceramics

The X-ray diffraction patterns of $Ba_{1-x}Sr_xTiO_3$ at room temperature are shown in Fig.9a. A single phase was observed for all the samples, suggesting that $BaTiO_3$ and $SrTiO_3$ form a complete solid solution for the studied x range. For x=0.3 the structure is tetragonal (space group *P4mm*) while it is cubic for x=0.35, 0.4, 0.45, 0.5 (space group *Pm3m*). Influence of the composition x on 110 and 220 X-ray diffraction lines of the perovskite type elementary cell is shown in Fig. 9b. One can see a peak broadening as the composition x increases. Moreover a shift of the diffraction lines to higher 2 values with increasing x can be seen in Fig.9b.

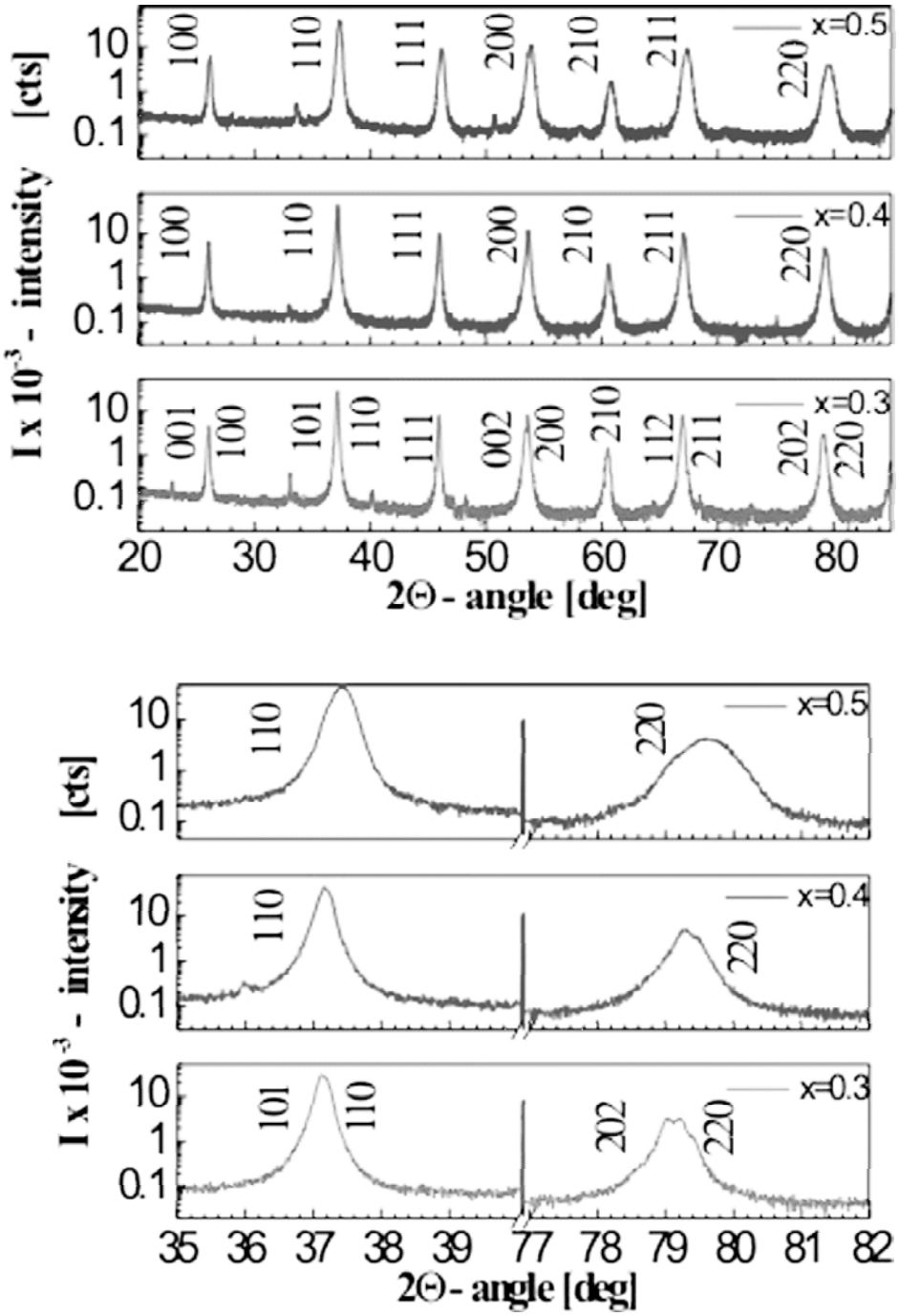

Fig. 9. a) X-ray diffraction patterns for $Ba_{1-x}Sr_xTiO_3$ compositions. b) X-ray diffraction lines 110 and 220 for $Ba_{1-x}Sr_xTiO_3$ compositions

An indication of a decrease of the unit cell volume with increasing x is shown in Fig.10 where the dependence of the average lattice constant $\langle a \rangle$ on composition x is given. For x=0.3 $\langle a \rangle = (a^2c)^{1/3}$ is taken where a and c are the tetragonal unit cell parameters.

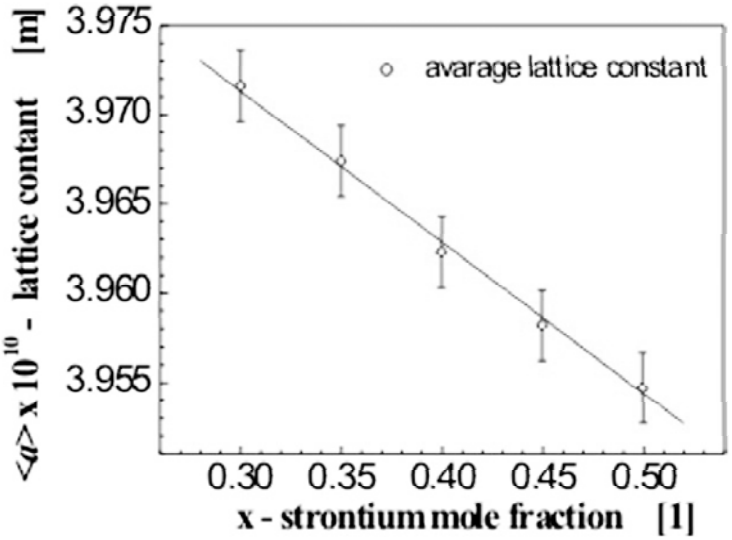

Fig. 10. Dependence of the average lattice constant $< a >$ on concentration x for $Ba_{1-x}Sr_xTiO_3$ solid solution

Figure 11 shows the curves of dielectric permittivity versus temperature for $Ba_{1-x}Sr_xTiO_3$ with various compositions $0.3 \leqslant \times \leqslant 0.5$. It can be seen from Fig.11 that the permittivity maxima temperatures shift to lower temperatures as x increases. For x=0.4 three peaks originated from cubic-tetragonal, tetragonal-orthorhombic and orthorhombic-rhombohedral phase transition can be seen.

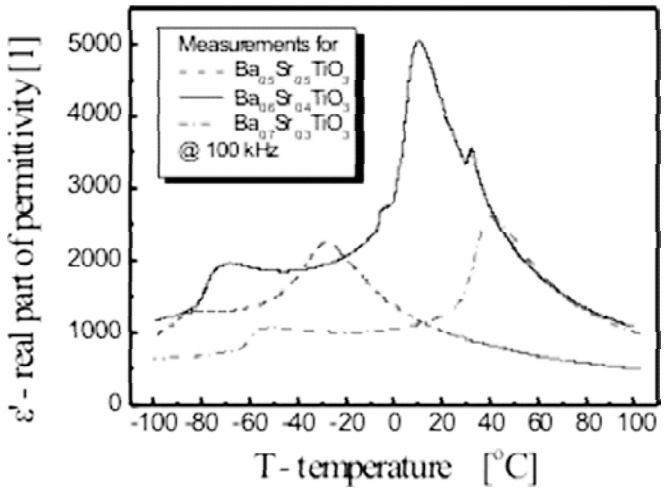

Fig. 11. Temperature dependence of the dielectric permittivity (ε') in the temperature range of the ferroelectric-paraelectric phase transition for BST with x=0.30, x=0.40, x=0.50 composition

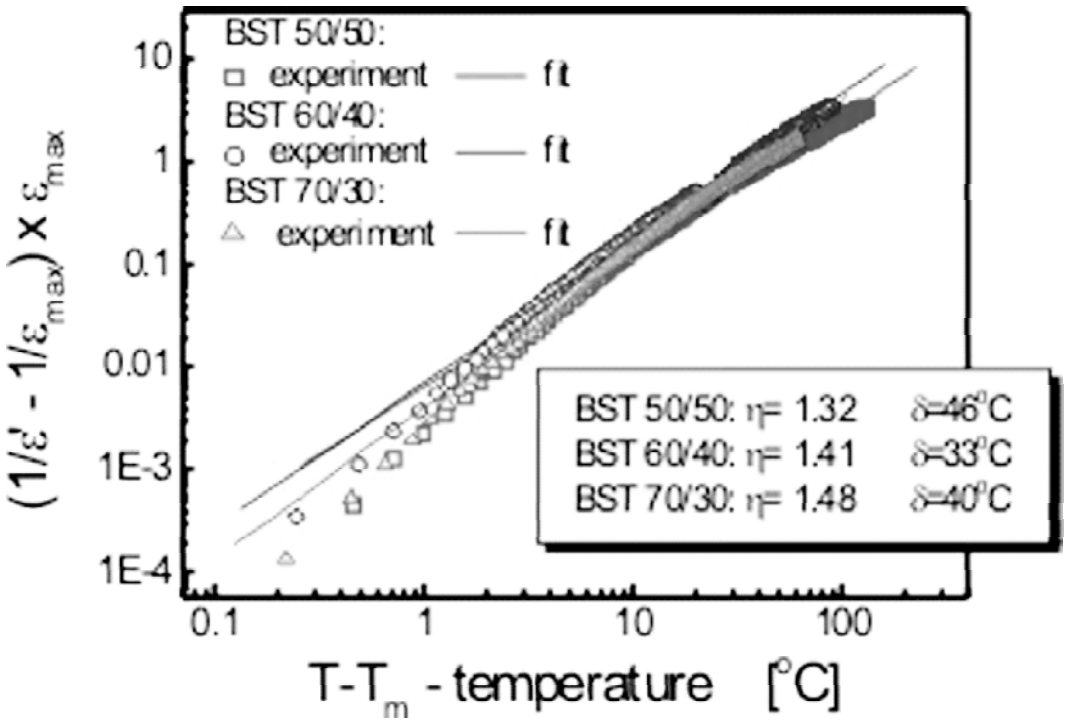

Fig. 12. Results of calculation of parameters η and δ for the diffused phase transition

Analysis of the dielectric permittivity data was done with the modified empirical equation Eq.1 [7]:

$$\varepsilon' = \frac{\varepsilon_m}{1 + ((T - T_m)/\delta)^{\eta}}. \quad (1)$$

The coefficient η gives information on the character of the phase transition. The parameter δ has the dimension of a temperature and indicates the range of temperature extension for the diffused phase transition. Results of calculations according Eq.1 are given in Fig.12.

The values of these parameters as obtained by fitting the dielectric data are: η=1.32 and δ=46°C for x=0.5, and η=1.41 and δ=33°C for x=0.4, and η=1.48 and δ=40°C for x=0.3.

4. Summary

Increasing the Sr^{+2} concentrations in the $BaTiO_3$-$SrTiO_3$ solid solutions linearly decreases the lattice constant. Temperature of the maximum dielectric permittivity T_m decreases with increasing x value. The values of parameters η and δ show that the sol-gel derived ceramics investigated in the present study exhibit mixed ferroelectric/relaxor character.

Acknowledgements

The authors wish to acknowledge Polish Ministry of Education and Science for financially supporting the present research from the funds for science in 2006-2009 as a research project N507 098 31/2319.

REFERENCES

[1] L. Zhou, P. M. Vilarinho, J. L. Baptista, Journal of the European Ceramic Society **19**, 2015-2019 (1999).
[2] W. Yang, A. Chang, B. Yang, Journal of Materials. Synthesis and Processing **10**, 303-311 (2003).
[3] M. Dekker, Handbook of nanophase materials, edited by Avery N.Goldstein, New York, Basel, Hong Kong, (1997).
[4] G. Nolze, W. Kraus, Powder Diffraction **13**(4), 256 (1998).
[5] J. Ryś, Stereologia materiałów, Fotobit Design, Kraków, (1995).

[6] S. B. Majumder, M. Jain, A. Martinez, R. S. Katiyar, F. W. Van Keuls, F. A. Miranda, Journal of Applied Physics **90**(2), 896-903 (2001).

[7] L. Kozielski, M. Adamczyk, A. Lisinska-Czekaj, T. Orkisz, M. Piechowiak, D. Czekaj, Phase Transitions **79**, 427-435 (2006).

Received: 10 September 2009.